IEEE Photonics Journal
An IEEE Photonics Society Publication

Open Access

Analysis of OAM Mode Purity of Integrated Optical Vortex Beam Emitters

Volume 9, Number 1, February 2017

Changzheng Sun, *Member, IEEE*
Juan Zhang
Bing Xiong
Jian Wang
Zhibiao Hao
Lai Wang
Yanjun Han
Hongtao Li
Yi Luo

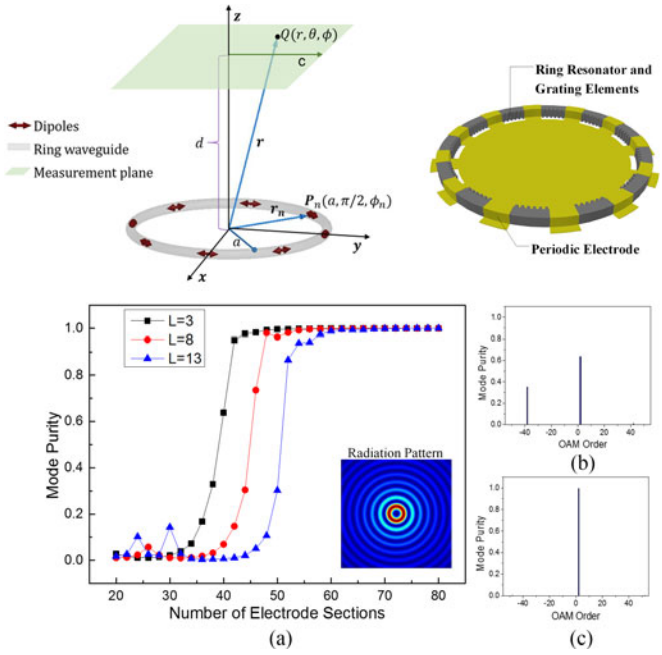

DOI: 10.1109/JPHOT.2017.2652722
1943-0655 © 2017 IEEE

Analysis of OAM Mode Purity of Integrated Optical Vortex Beam Emitters

Changzheng Sun, *Member, IEEE*, Juan Zhang, Bing Xiong, Jian Wang, Zhibiao Hao, Lai Wang, Yanjun Han, Hongtao Li, and Yi Luo

Laboratory for Information Science and Technology, State Key Laboratory on Integrated Optoelectronics, Department of Electronic Engineering, Tsinghua University, Beijing 100084, China

DOI:10.1109/JPHOT.2017.2652722

Manuscript received October 23, 2016; revised January 7, 2017; accepted January 9, 2017. Date of publication January 16, 2017; date of current version January 27, 2017. This work was supported by the National Basic Research Program of China under Grant 2012CB315605 and Grant 2014CB340002; by the National Natural Science Foundation of China under Grant 61210014, Grant 61321004, Grant 61307024, Grant 61574082, and Grant 51561165012; by the High Technology Research and Development Program of China under Grant 2015AA017101; by Tsinghua University Initiative Scientific Research Program under Grant 20131089364, Grant 20161080068, and Grant 20161080062; and by the Open Fund of State Key Laboratory on Integrated Optoelectronics under Grant IOSKL2014KF09.
Corresponding author: J. Zhang (e-mail: zhangjuan13@mails.tsinghua.edu.cn).

Abstract: A theoretical analysis is presented to investigate the orbital angular momentum (OAM) mode purity of microring-resonator-based integrated optical vortex emitters. By extending the dipole model for integrated vortex emitters, the influence of optical losses and grating imperfections on OAM mode purity of the output beam is investigated, thus clarifying the mode purity performance of the device in many practical scenarios. This work provides an efficient tool for the design of emitters with high OAM mode purity for optical communications or quantum information processing.

Index Terms: Optical vortices, integrated optics devices.

1. Introduction

Recently, optical beams carrying orbital angular momentum (OAM) [1] have attracted much attention, due to their potential to enhance fiber network capacity [2], as well as enabling high dimensional quantum information processing [3]. Emitters capable of generating OAM carrying beams are of particular importance in such applications. Among the various devices proposed and demonstrated for this purpose [4]–[7], the integrated vortex beam emitters incorporating angular gratings in microring resonators are of particular interest, as their compactness lends themselves directly to large-scale integration [4]. Much effort has been devoted to the understanding of the behavior of such devices, e.g., the near and far zone beam patterns [8], spin-orbital interactions of angular momentum [9], and switching between OAM modes [10]. In this work, we present a detailed analysis of the OAM mode purity of the integrated vortex emitter, which is of great importance for both classical and quantum applications. The dipole model developed in [8] is extended to account for the influence of optical loss and grating imperfections. Our analysis is believed to provide valuable insight for the design and realization of vortex beam emitters with high OAM mode purity.

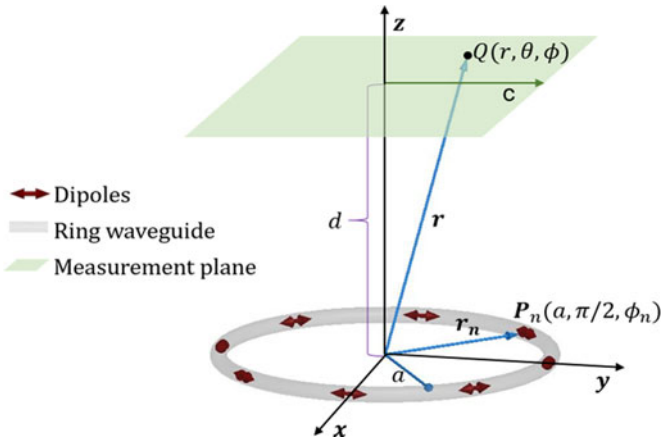

Fig. 1. Dipole model for integrated vortex beam emitter.

2. Analysis Model for Integrated Vortex Emitters

To investigate the far-field beam property of the integrated optical vortex emitter, we adopt the theoretical model proposed in [8], in which the grating induced scattering is described by a series of azimuthally polarized dipole oscillators, as shown in Fig. 1. Supposing that the number of total grating elements is N, and that the light in the microring has an azimuthal resonant order of M, there will be a phase difference of $2\pi l/N$ between adjacent dipoles, with $l = M - N$ being an integer [8]. The paraxial radiation field at a point (r, θ, ϕ) on the measurement plane, which is assumed to be far from the microring, i.e. $d \gg a$, is given by [8]

$$\boldsymbol{E} = -\frac{k^2 \exp(jkr)}{4\pi\varepsilon_0 r} \sum_{n=1}^{N} \exp[jak \sin\theta \cos(\phi_n - \phi)]\boldsymbol{p_n} \tag{1}$$

where d is the distance between the measurement plane and the device, k is the wave number in vacuum, a is the microring radius, and $\boldsymbol{p_n} = p_0(\sin\phi_n \hat{\boldsymbol{x}} - \cos\phi_n \hat{\boldsymbol{y}}) \exp(j\varphi_n)$ is the n-th dipole moment, with $\varphi_n = 2\pi nl/N$ and $\phi_n = 2\pi n/N$ describing its phase and azimuthal position. Here, for the moment, all dipoles are assumed to have an equal amplitude of p_0.

By defining $E_0 = k^2 p_0 \exp(jkr)/(4\pi\varepsilon_0 r)$ and $\beta = ak \sin\theta$, the x component of the radiation field can be expressed as

$$\begin{aligned} E_x &= E_0 \sum_{n=1}^{N} \exp[j\beta \cos(\phi_n - \phi)] \exp(jl\phi_n) \sin\phi_n \\ &= E_x^+ + E_x^- \end{aligned} \tag{2}$$

where $E_x^{\pm}$ are given by

$$E_x^{\pm} = \frac{\pm E_0}{2j} \sum_{n=1}^{N} \exp[j\beta \cos(\phi_n - \phi)] \exp[j(l \pm 1)\phi_n]. \tag{3}$$

3. Influence of Grating Element Number

3.1 Infinite Number of Grating Elements

First, we consider the case that the number of dipole N is very large, and therefore, the sum in (3) can be cast into an integral, i.e.,

$$E_x^{\pm} = \frac{\pm E_0}{2j} \int_0^{2\pi} \exp[j\beta \cos(\varphi - \phi)] \exp[j(l \pm 1)\varphi] \frac{N}{2\pi} d\varphi \tag{4}$$

which, in passing, is similar to the paraxial radiation field of a circular traveling-wave antenna [11]. With the help of Jacobi-Anger expansion [12]

$$\exp(jz\cos\theta) = \sum_{m=-\infty}^{+\infty} j^m J_m(z)\exp(jm\theta) \tag{5}$$

(4) can be cast into the following form:

$$E_x^{\pm} = \frac{\pm NE_0}{4\pi j}\sum_{m=-\infty}^{+\infty} j^m J_m(\beta)\exp(jm\phi)\cdot\int_0^{2\pi}\exp(-jm\varphi)\exp[j(l\pm 1)\varphi]d\varphi = \frac{j^l NE_0}{2}J_{l\pm 1}(\beta)\exp[j(l\pm 1)\phi] \tag{6}$$

As a result, the radiation field is found to be

$$\boldsymbol{E} = \begin{bmatrix} E_x \\ E_y \end{bmatrix} = E_c J_{l-1}(\beta)\exp[j(l-1)\phi]\begin{bmatrix} 1 \\ j \end{bmatrix} + E_c J_{l+1}(\beta)\exp[j(l+1)\phi]\begin{bmatrix} 1 \\ -j \end{bmatrix} \tag{7}$$

where $E_c = j^l NE_0/2$ is a value independent of θ and ϕ.

It is readily recognized that the field consists of two circularly polarized OAM beams rotating in opposite directions, each carrying a topological charge of $l-1$ and $l+1$, respectively. In applications where a pure OAM mode is desirable, a polarization filter can be used to select one of the two OAM modes [10]. For the sake of clarity, in the discussion of OAM mode purity given below, only left hand circularly polarized (LHCP) OAM modes are considered, corresponding to $\boldsymbol{E}^-$.

3.2 Finite Number of Grating Elements

The number of grating elements in an actual device is always limited, and the beam pattern for a finite number of dipoles can be obtained from (3) and (5)

$$\begin{aligned} E_x^- &= \frac{E_0}{2j}\sum_{m=-\infty}^{+\infty} j^m J_m(\beta)\exp(jm\phi)\cdot\sum_{n=1}^{N}\exp\{-j[m-(L-1)]\phi_n\} \\ &= \frac{NE_0}{2j}\sum_{k=-\infty}^{+\infty} j^{kN+l-1}J_{kN+l-1}(\beta)\exp[j(kN+l-1)\phi]. \end{aligned} \tag{8}$$

Equation (8) reveals a striking feature of the field emitted by a vortex beam emitter with finite number of grating elements: It is not a pure OAM mode but a sum of OAM beams with different topological charges. In addition, only N distinct field patterns can be obtained by varying the value of l. The limited number of output pattern available for finite number of radiation elements has been pointed out in previous study [13]. However, to our knowledge, it is the first time that it is explicitly stated that each pattern actually corresponds to a combination of mixed OAM modes.

Fig. 2 shows the simulation results obtained with a ring radius $a = 40\ \mu$m and $\lambda = 1.55\ \mu$m. Here, OAM mode purity is defined as the ratio between the power of the OAM mode with topological charge $l-1$ to that of the entire beam. To comply to paraxial approximation, the maximum divergence angle is limited to $\tan\theta = 0.1$ in our simulations. Experimentally, this can be implemented by an aperture to filter out the nonparaxial light. Mathematically, limiting the angle θ helps circumvent the divergence of the integral involving Bessel functions. In our simulation, Bessel beams with an order higher than 200 are neglected because of their large divergence angle. The field at the measurement plane, which is placed at a distance of $d = 1$ mm from the device, is calculated with a step size of 0.5 μm along x and y directions. As is evident from Fig. 2, to improve mode purity of the vortex beam emitter, it is crucial to increase the number of grating elements while keeping $|l| \ll N/2$. This can be readily explained with the help of (8). Since $J_n(\beta) \sim (\beta/2)^n/n!$ for small β, the $l-1$ mode dominates when N is fairly large and $|l| \ll N/2$. On the other hand, for l close to $N/2$, the $l-1$ and $(l-1)-N$ components have comparable amplitudes, leading to a significantly degraded OAM mode purity.

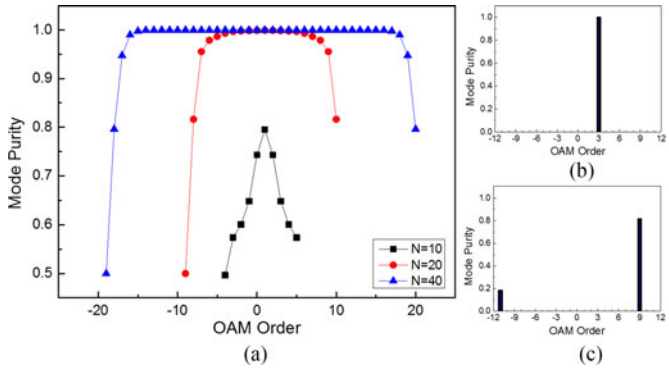

Fig. 2. Influence of finite grating element number on OAM mode purity. (a) Variation of OAM mode purity as a function of l for a given number of grating elements N. (b) and (c) Typical mode spectra for $l \ll N$ and $l \sim N/2$, respectively.

4. Variation in Radiation Strength Along the Ring

Now, we consider the case where the dipole amplitude varies along the ring resonator, which may be induced by absorption in the waveguide, scattering by the grating elements, or imperfection of gratings. Such variation in dipole amplitude can be described by an amplitude modulation function $F_n(\phi_n)$, i.e., $p_n = p_0 F_n(\phi_n)$.

In the following analysis, we shall assume a sufficiently large number of grating elements, so that the radiation field is given by the integral shown in (4). Under such assumption, the modulation function $F_n(\phi_n)$ turns into a continuous function $F(\varphi)$, and the radiation field is given by

$$E_x^- = A \int_0^{2\pi} F(\varphi) \exp[j\beta \cos(\varphi - \phi)] \exp[j(l-1)\varphi] d\varphi \tag{9}$$

where A is a constant. It is recognized that $F(\varphi)$ is periodic, i.e., $F(\varphi + 2\pi) = F(\varphi)$. As a result, it can be expanded into the sum of Fourier components

$$F(\varphi) = \sum_{m=-\infty}^{+\infty} F_m \exp(-jm\varphi) \tag{10}$$

where the Fourier coefficient F_m is given by

$$F_m = \frac{1}{2\pi} \int_0^{2\pi} F(\varphi) \exp(jm\varphi) d\varphi. \tag{11}$$

Inserting (10) into (9) and invoking the Jacobi-Anger expansion given in (5), we have

$$\boldsymbol{E}^- = E_c \sum_{m=-\infty}^{+\infty} j^{-m} J_{l-1-m}(\beta) F_m \exp[j(l-1-m)\phi] \begin{bmatrix} 1 \\ j \end{bmatrix}. \tag{12}$$

The above result indicates that modulation of the dipole amplitude results in a spreading of topological charge values. If $F(\varphi)$ is a slow varying function, with Fourier components F_m only significant for small $|m|$, the resultant radiation field would contain angular momentum clustered around $l-1$. On the other hand, if $F(\varphi)$ is a periodic function with Fourier component $F_{\pm m}$ dominant, the angular momentum of the radiation field would center around $(l-1) \pm m$.

4.1 Optical Loss

Bearing the above general discussion in mind, we now turn to some practical scenarios. First, we shall consider OAM purity in the presence of optical loss in the ring waveguide. The modulation

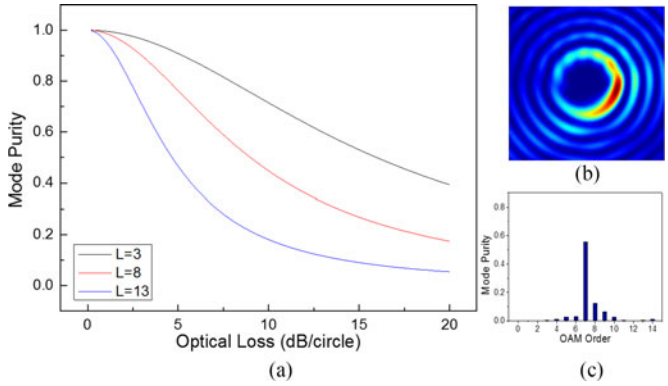

Fig. 3. (a) Mode purity as a function of loss within the microring. (b) Radiation pattern and (c) OAM mode spectrum for $l = 8$ with a loss of 8 dB/circle.

function is given by $F(\varphi) = \exp(-\gamma a\varphi)$, where γ is the loss coefficient. It is readily found that

$$F_m = \frac{1 - \exp(-\gamma 2\pi a)}{2\pi(\gamma a - jm)}. \tag{13}$$

Fig. 3 shows the simulation results with $a = 100$ μm (the other parameters are the same as in Section 3). A larger microring radius is adopted in Section 4 to accommodate a sufficiently large number of grating elements. It is seen that the mode purity deteriorates with increasing optical loss coefficient γ. Furthermore, the degradation in OAM mode purity becomes more pronounced when it comes to high order OAM beams.

One possible method to mitigate the loss induced OAM purity degradation is to gradually increase the size of the grating elements along the ring [14]. In this way, a uniform dipole amplitude may be maintained, as the decreasing optical intensity along the waveguide is compensated by the increased scattering by the downstream grating elements.

4.2 Partially Obscured Gratings

Another case that is of particular interest is when part of the gratings is obscured or damaged. This may also happen when the vortex beam emitter is to be fabricated on InP based materials to form active OAM devices. By injecting current into the microring, it is possible to compensate the loss due to absorption and scattering. However, the metal electrode for current injection would obscure part of the gratings.

Considering the case that only a portion of gratings are obscured, the corresponding modulation function is

$$F(\varphi) = \begin{cases} 0, & -\eta\pi < \eta < \pi \\ 1, & \text{otherwise} \end{cases} \tag{14}$$

where η is the portion of obscured grating. Consequently, the Fourier coefficient F_m is

$$F_m = \begin{cases} \dfrac{\sin m\pi(1-\eta)}{m\pi}, & m \neq 0 \\ 1 - \eta, & m = 0. \end{cases} \tag{15}$$

As revealed by the simulation results given in Fig. 4, when the gratings are partially obscured, side OAM modes show up around the dominant $l - 1$ mode. Actually, if we take partially obscuring the grating to be the same as blocking a sector of the output OAM beam, the appearance of side OAM modes is simply a result of angular Heisenberg uncertainty principle [3].

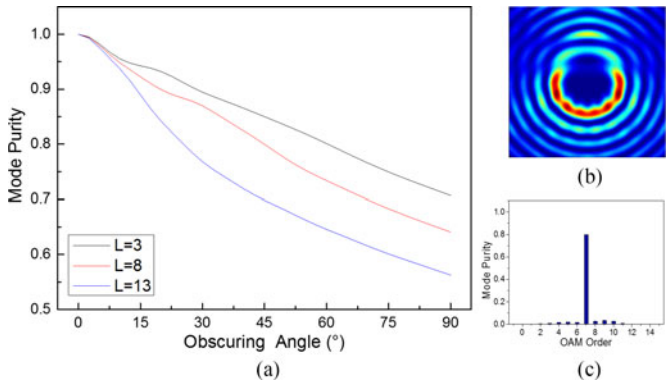

Fig. 4. (a) OAM mode purity for partially obscured gratings. (b) Radiation pattern and (c) OAM mode spectrum for $l = 8$ and $\eta = 1/8$.

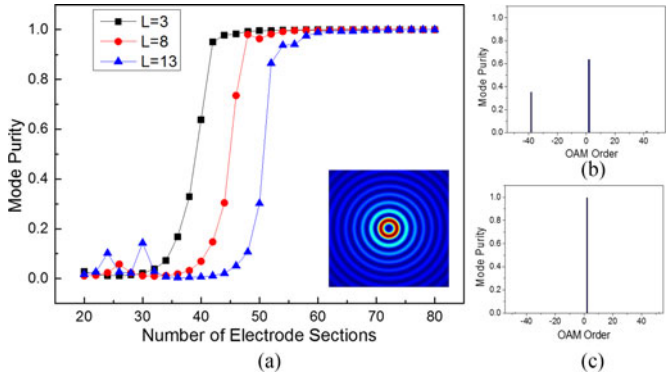

Fig. 5. (a) OAM mode purity for periodically obscured gratings. (Inset) Radiation pattern for $s = 50$. OAM mode spectra for $l = 3$ when (b) $s = 40$ and (c) $s = 50$.

4.3 Periodically Obscured Gratings

When only a portion of the gratings is obscured by the electrode, output beam is no longer circularly symmetric, and degraded OAM purity ensues. Circular symmetry can be preserved by adopting a periodic electrode along the microring, which corresponds to a modulation function of the form

$$F(\varphi) = \begin{cases} 0, & \text{for } \dfrac{(4p-1)\pi}{2s} \le \varphi < \dfrac{(4p+1)\pi}{2s} \\ 1, & \text{for } \dfrac{(4p+1)\pi}{2s} \le \varphi < \dfrac{(4p+3)\pi}{2s} \end{cases} \tag{16}$$

where s is the number of total electrode sections.

The radiation field is

$$\boldsymbol{E}^- = E_c \sum_{m=-\infty}^{+\infty} j^{-ms} J_{l-1-ms}(\beta) F_m \exp[j(l-1-ms)\phi] \begin{bmatrix} 1 \\ j \end{bmatrix} \tag{17}$$

with the Fourier coefficient F_m given by

$$F_m = \begin{cases} \dfrac{\sin m\pi/2}{m\pi}, & m \neq 0 \\ 1/2, & m = 0. \end{cases} \tag{18}$$

Periodically obscuring the gratings causes OAM modes with topological charge $(l-1)\pm ms$ to show up in addition to the original dominant $l-1$ mode. Nevertheless, if the number of electrode sections s is large enough, the coefficient $J_{l-1\pm s}(\beta)$ can be ignored for small β, which means a small beam divergence angle θ. Consequently, high OAM mode purity can be maintained even though the gratings are obscured periodically, as confirmed by the simulation results shown in Fig. 5.

5. Conclusion

In summary, we have presented a detailed study on OAM mode purity of integrated vortex beam emitters. By introducing the amplitude modulation function into the dipole model and performing subsequent Fourier expansion, OAM mode purity in the presence of optical loss or grating imperfections is analyzed. Though representing grating elements by dipole oscillators is only valid for vortex beam emitters with narrow grating elements [8], it can be extended to more general cases with the help of diffraction theory. Furthermore, the results obtained in this study are believed to provide a useful guideline to the design of other types of OAM emitters. To obtain OAM beam with high mode purity, the number of radiation elements N, which can be radial grating teeth [4], second order gratings [5], [6], or simply waveguide ends [7], must be large enough, so that $N \gg l$. Furthermore, in addition to maintaining a correct phase difference between adjacent radiation elements, a uniform or symmetric emission intensity is also essential to high OAM mode purity.

Acknowledgment

The authors would like to thank Profs. S. Yu and X. Cai of Sun Yat-Sen University for fruitful discussions.

References

[1] A. E. Willner *et al.*, "Optical communications using orbital angular momentum beams," *Adv. Opt. Photon.*, vol. 7, no. 1, pp. 66–106, 2015.
[2] A. M. Yao and M. J. Padgett, "Orbital angular momentum: Origins, behavior and applications," *Adv. Opt. Photon.*, vol. 3, no. 2, pp. 161–204, 2011.
[3] S. Franke-Arnold, L. Allen, and M. Padgett, "Advances in optical angular momentum," *Laser Photon. Rev.*, vol. 2, no. 4, pp. 299–313, 2008.
[4] X. Cai *et al.*, "Integrated compact optical vortex beam emitters," *Science*, vol. 338, no. 6105, pp. 363–366, 2012.
[5] C. R. Doerr and L. L. Buhl, "Circular grating coupler for creating focused azimuthally and radially polarized beams," *Opt. Lett.*, vol. 36, no. 7, pp. 1209–1211, 2011.
[6] D. Zhang, X. Feng, Y. Huang, "Encoding and decoding of orbital angular momentum for wireless optical interconnects on chip," *Opt. Exp.*, vol. 20, no. 24, pp. 26986–26995, 2012.
[7] B. Guan *et al.*, "Free-space coherent optical communication with orbital angular, momentum multiplexing /demultiplexing using a hybrid 3D photonic integrated circuit," *Opt. Exp.*, vol. 22, no. 1, pp. 145–156, 2014.
[8] J. Zhu, X. Cai, Y. Chen, and S. Yu, "Theoretical model for angular grating-based integrated optical vortex beam emitters," *Opt. Lett.*, vol. 38, no. 8, pp. 1343–1345, 2013.
[9] J. Zhu, Y. Chen, Y. Zhang, X. Cai, and S. Yu, "Spin and orbital angular momentum and their conversion in cylindrical vector vortices," *Opt. Lett.*, vol. 39, no. 15, pp. 4435–4438, 2013.
[10] M. J. Strain *et al.*, "Fast electrical switching of orbital angular momentum modes using ultra-compact integrated vortex emitters," *Nature Commun.*, vol. 5, 2014, Art. no. 4856.
[11] Z. Zhang, S. Zheng, Y. Chen, X. Jin, H. Chi, and X. Zhang, "The capacity gain of orbital angular momentum based multiple-input-multiple-output system," *Sci. Rep.*, vol. 6, 2016, Art. no. 25418.
[12] G. N. Watson, "The Bessel coefficients" in *A Treatise on the Theory of Bessel Functions*. Cambridge, U.K.: Cambridge Univ. Press, 1952, p. 22.
[13] B. Thide *et al.*, "Utilization of photon orbital angular momentum in the low-frequency radio domain," *Phys. Rev. Lett.*, vol. 99, 2007, Art. no. 087701.
[14] S. Yu, X. Cai, and N. Zhang, "High index contrast integrated optics in the cylindrical coordinate," *Proc. SPIE*, vol. 9372, 2015, Art. no. 937203.